The AstroSat UV Deep Field South – III. Evolution of the UV luminosity function and luminosity density from $z \sim 0.8$–0.4

Souradeep Bhattacharya [1,2]★ and Kanak Saha[2]

[1]*Centre for Astrophysics Research, Department of Physics, Astronomy and Mathematics, University of Hertfordshire, Hatfield AL10 9AB, UK*
[2]*Inter University Centre for Astronomy and Astrophysics, Ganeshkhind, Post Bag 4, Pune 411007, India*

ABSTRACT

We characterize the rest-frame 1500 Å UV luminosity function (UVLF) from deep AstroSat/UV Imaging Telescope (UVIT) F154W and N242W imaging in the Great Observatories Origins Survey South (GOODS-S) deep field. The UVLFs are constructed and subsequently characterized with fitted Schechter function parameters from Far-UV (FUV) observations at $z < 0.13$ and Near-UV (NUV) observations in seven redshift bins in $z \sim 0.8$–0.4. The UVLF slope (α) and characteristic magnitude (M^*) are consistent with previous determinations for this redshift range based on AstroSat/UVIT GOODS-North observations, as well as with those from *Galaxy evolution Explorer* and *Hubble Space Telescope* observations. However, differences in the normalization factor (ϕ_*) are present for UVLFs for some redshift bins. We compute the UV luminosity density, ρ_{UV}, combining our determined UVLF parameters with literature determinations out to $z \sim 10$. The ρ_{UV} trend with redshift implies the rapid increase in cosmic star formation till its peak at $z \sim 3$ (cosmic noon) followed by a slow decline till present day. Both the initial increase in cosmic star formation and subsequent decline are found to be more rapid than previous determinations.

Key words: galaxies: evolution – galaxies: luminosity function, mass function – galaxies: star formation – ultraviolet: galaxies.

1 INTRODUCTION

Quantifying the distribution of luminosities within a given population, galaxy luminosity functions are key probes into the underlying physical processes that govern galaxy formation and evolution (see review by Johnston 2011). The rest-frame 1500 Å UV luminosity function (UVLF), sensitive to ongoing star formation in galaxies (Wyder et al. 2005), offers insights into the star formation activity of galaxies across cosmic time.

The UVLF is typically characterized within a given redshift range with the classic Schechter function (Schechter 1976) parametrized in the following manner as a function of magnitude M:

$$\phi(M)\mathrm{d}M = \frac{ln(10)}{2.5} \, \phi_* \, (10^{0.4\Delta M})^{\alpha+1} e^{-10^{0.4\Delta M}} \mathrm{d}M, \tag{1}$$

where $\Delta M = M^* - M$, ϕ_* is a normalization factor which defines the overall density of galaxies (number per cubic Mpc), M^* is the characteristic galaxy magnitude, and α defines the faint-end slope (typically negative implying large numbers of relatively passive galaxies with low luminosities).

The UVLF has been extensively characterized at $z \sim 1$–9 from *Hubble Space Telescope* (*HST*) surveys in deep-fields[1] (e.g. Oesch et al. 2010; Finkelstein et al. 2015; Alavi et al. 2016; Bouwens et al. 2022) and at $z > 8$ from recent *JWST* deep-field observations (e.g. Bouwens et al. 2023; Finkelstein et al. 2024). However, at $z < 1$

which spans a wide range of ages (~ 8 Gyr), direct UVLF characterization has been more limited to relatively bright sources from *Galaxy evolution Explorer* (*GALEX*; Arnouts et al. 2005; Wyder et al. 2005), *Swift UV/Optical Telescope* (UVOT; Hagen et al. 2015), and *XMM–Newton* Optical Monitor (XMM-OM; Page et al. 2021; Sharma, Page & Breeveld 2022; Sharma et al. 2024) observations, as well as earlier ones from balloon-borne observations (Treyer et al. 1998; Sullivan et al. 2000). The preferential observations of bright sources is due to relatively low angular resolution of near-UV (NUV) channels for the aforementioned telescopes (FWHM$_{NUV,GALEX}$ = 5.3 arcsec; FWHM$_{NUV,UVOT}$ = 2.5 arcsec; FWHM$_{NUV,XMM-OM}$ = 2 arcsec) adversely affecting the detection of faint sources in crowded deep fields.

The UV Imaging Telescope (UVIT; Kumar et al. 2012) onboard *AstroSat* (Singh et al. 2014) recently carried out higher angular-resolution (FWHM$_{F154W}$ = 1.18 arcsec, FWHM$_{N242W}$ = 1.11 arcsec) UV observations of the Great Observatories Origins Deep Survey – North and South deep fields (GOODS-N and GOODS-S respectively; Giavalisco et al. 2004). The observations of the GOODS-N field are described in Mondal et al. (2023). In Bhattacharya, Saha & Mondal (2024, hereafter Bh+24), we presented UVLFs for $z <= 0.13$ for a single bin and for $0.378 < z < 0.768$ for seven bins (bin size ~ 0.055 in z), thereby characterizing the UVLF in the GOODS-N field with unprecedented resolution in redshift and thus probing the variation of the fitted UVLF parameters over ~ 2.7 Gyr in age. We found that α was at its steepest at $z \sim 0.63$, potentially implying highest star-formation at this instant with galaxies being relatively more passive before and after this time within the probed redshift range.

Our recent UV observations of the GOODS-S deep field with AstroSat/UVIT (Saha et al. 2024), deeper than those in the GOODS-N

★ E-mail: s.bhattacharya3@herts.ac.uk
[1]Sensitive observations over a small region of the sky that provide unique opportunities to detect and analyse faint, low-luminosity galaxies.

field allow us to probe the behaviour of the fitted UVLF parameters in an additional field, and draw potentially more universally applicable inferences on cosmic star-formation at $z \sim 0.4$–0.8. Furthermore, from the UVLF parameters thus determined at low-z and given the availability of fitted UVLF parameters out to $z \sim 10$, the behaviour of cosmic star-formation may be analysed from computing the UV luminosity density (e.g. Oesch et al. 2010; Alavi et al. 2016) over this large redshift range.

We describe the AstroSat/UVIT GOODS-S data and associated photometric redshift utilized in this work in Section 2. The constructed UVLFs are described in Section 3. We discuss the consistency of the fitted UVLF parameters with past determinations in Section 4 along with the evolution of the UV luminosity density. We conclude in Section 5.

Throughout this paper, we use the standard cosmology ($\Omega_m = 0.3$, $\Omega_\Lambda = 0.7$ with $H_0 = 70$ km s^{-1} Mpc^{-1}). Magnitudes are given in the AB system (Oke 1974).

2 GALAXY CATALOGUE DATA

In Saha et al. (2024), we present deep UV imaging observations of the GOODS-S field with AstroSat/UVIT (AstroSat UV Deep Field South, hereafter AUDFs), using one FUV (F154W) and one NUV filter (N242W). The deep and shallow parts of AUDFs have exposure times of $\sim$62 000 s ($\sim$64 000 s) and $\sim$31 000 s ($\sim$34 000 s) respectively in F154W (N242W). This imaging covered $\sim$236 sq. arcmin, including $\sim$193 sq. arcmin covered by the *HST* CANDELS survey with multiple *HST* filters (Grogin et al. 2011, Koekemoer et al. 2011) and 43.4 sq. arcmin spanned by the Hubble Deep UV Legacy Survey in the GOODS-S field (HDUV-S) with *HST* F275W and F336W filters (Oesch et al. 2018).

As was the case for AUDFn (see Bh+24 for details), we utilize only those F154W and N242W sources catalogued by Saha et al. (2024) that have a single unique *HST* counterpart within 1.4 arcsec. We additionally restrict ourselves to only those sources that are brighter than the 50 per cent completeness limits of 27.63 (27.3) and 27.04 (26.73) mag for the deep (shallow) N242W and F154W images, respectively. The redshifts for our galaxies were adopted from the z_{best} value of the CANDELS Photometric Redshift Catalogue (Kodra et al. 2023). We utilize only those galaxies to construct the rest-frame 1500 Å UVLFs that are at $z <= 0.13$ and $0.378 < z < 0.768$ in the F154W and N242W filters respectively, where they are most sensitive to the redshifted 1500 Å as per their filter transmission functions (Tandon et al. 2020). We thus select 200 and 2067 sources with only a single *HST* counterpart in the F154W and N242W images respectively within these redshift ranges.

Additionally, we utilize the *HST* F275W photometric catalogue from HDUV-S (Oesch et al. 2018) to construct UVLFs for galaxies at $0.679 < z < 0.79$ as a consistency check to the N242W based UVLFs. There are 298 galaxies in this redshift range observed in F275W filter down to the 5σ detection limit of 27.6 mag (Oesch et al. 2018).

The presence of any active galactic nuclei (AGN), especially bright ones ($M_{1500} < -19$ mag), may affect the determined parameters of the UVLF. The presence of faint AGN is expected to only negligibly affect the fitted UVLF parameters at this redshift range (Bh+24). Lyu et al. (2022) presented a catalogue of 901 AGN identified in the GOODS-S region using diagnostics covering X-ray to radio observations. Of these 11, 120 and 19 have counterparts in the redshift ranges of interest for the aforementioned F154W, N242W, and F275W sources, respectively. As we found many of these (none in F154W but 31 in N242W, and five in F275W) to have
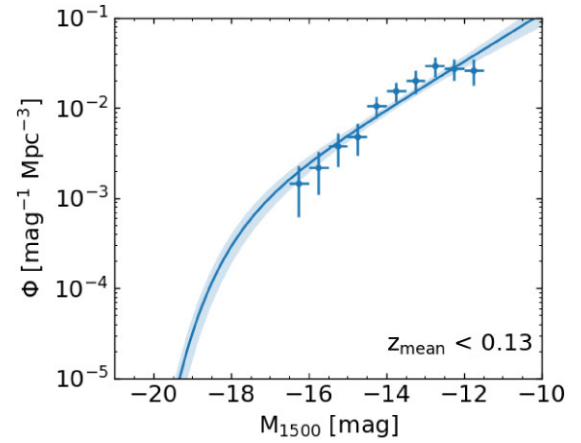
Figure 1. The 1500 Å LF at $z < 0.13$ from the F154W imaging of the GOODS-S field. The Schechter function fit is marked with a solid line, with the 1 σ uncertainty shaded.

$M_{1500} < -19$ mag (unlike in AUDFn; Bh+24), we have removed these known AGN from our sample before fitting the UVLFs.

3 THE UV (1500 Å) LUMINOSITY FUNCTIONS

The 1500 Å LF for $z <= 0.13$ for a single bin, $0.378 < z < 0.768$ for seven bins, and $0.679 < z < 0.79$ for two bins are fitted from the aforementioned observed number of galaxies in the F154W, N242W, and F275W filters, respectively. The procedure followed is the same as for AUDFn (Bh+24) which we describe briefly as follows:

(i) We carry out completeness correction based on the recovery fraction of sources as a function of apparent magnitude (see fig. 14 in Saha et al. 2024) that was done using artificial source injection (e.g. Bhattacharya et al. 2017, 2019) for each image.

(ii) Further corrections are applied to account for the fraction of total identified sources that have a unique *HST* counterpart as well as small K-corrections are derived from appropriate best-fitting templates.

(iii) We compute the luminosity distance of each galaxy, remove the known AGN, and construct the UVLF whose binned representation follows the method of Page & Carrera (2000).

(iv) The UVLF is then fitted with the classic Schechter function (Schechter 1976) using a maximum likelihood estimator fit.

For the F154W based UVLF at $z <= 0.13$ (see Fig. 1), galaxies are observed down to $M_{1500} = -11.5$ mag but there is a lack of bright galaxies ($M_{1500} > -16.5$ mag). We thus fix $M^* = -18.03$ (same value as Arnouts et al. 2005 from *GALEX* FUV data). The fitted ϕ_* and α values for the best-fitting Schechter function are noted in Table 1.

To construct the N242W based UVLFs at $0.378 < z < 0.768$, the observed galaxies are divided into seven equal bins in redshift ($\Delta z = 0.055$). The mean redshift of each bin, z_{mean}, the range of redshifts as well as the number of galaxies and AGN in each bin are noted in Table 1. The binned representation of the UVLFs for each redshift bin is shown in Fig. 2. The Schechter function is fitted to the UVLF in each redshift bin keeping α, ϕ_*, and M^* as free parameters. The best-fitting Schechter function parameters are noted in Table 1.

The galaxies from the HDUV-S sample (Oesch et al. 2018) are divided into two redshift bins ($\Delta z = 0.055$) at $0.679 < z < 0.79$. The binned representation of these UVLFs is shown in red in Fig. 2, but without any completeness correction (see section 3.4 in Bh+24

Table 1. Fitted UVLF parameters. Column 1: central redshift of each bin; column 2: range of redshifts spanned by each bin; column 3: no. of galaxies in each bin considered for UVLF fitting; column 4: no. of AGN removed in each bin; columns 5–7: fitted Schechter function parameters; column 8: logarithm of luminosity density.

| z_{mean}	z_{range}	No. of galaxies	No. of AGN	ϕ_* 10^{-3} mag^{-1} Mpc^{-3}	$M*$ mag	α	$\log(\rho_{UV})$ erg/s/Hz/Mpc^3
				AUDFs FUV			
0.1	0.01–0.13	189	11	0.91 ± 0.3	-18.03	-1.65 ± 0.08	25.17 ± 0.14
				AUDFs NUV			
0.41	0.378–0.434	189	5	1.85 ± 1.54	-18.51 ± 0.68	-1.54 ± 0.2	25.53 ± 0.45
0.46	0.434–0.489	157	3	4.19 ± 2.35	-17.97 ± 0.55	-1.13 ± 0.23	25.43 ± 0.33
0.52	0.489–0.545	274	14	5.11 ± 4.29	-18.36 ± 0.6	-1.27 ± 0.25	25.73 ± 0.44
0.57	0.545–0.601	269	13	7.55 ± 4.53	-17.94 ± 0.42	-1.32 ± 0.28	25.76 ± 0.31
0.63	0.601–0.657	320	16	4.23 ± 3.12	-18.79 ± 0.56	-1.37 ± 0.27	25.87 ± 0.39
0.68	0.657–0.712	347	36	9.73 ± 4.1	-18.59 ± 0.39	-0.96 ± 0.27	25.99 ± 0.46
0.74	0.712–0.768	387	33	10.94 ± 1.57	-18.55 ± 0.13	-0.94 ± 0.1	26.03 ± 0.08
				HDUV-S			
0.71	0.679–0.734	126	8	1.91 ± 0.99	-19.03 ± 0.46	-1.33 ± 0.16	25.57 ± 0.35
0.76	0.734–0.79	153	11	2.39 ± 1.0	-18.98 ± 0.4	-1.15 ± 0.16	25.6 ± 0.24
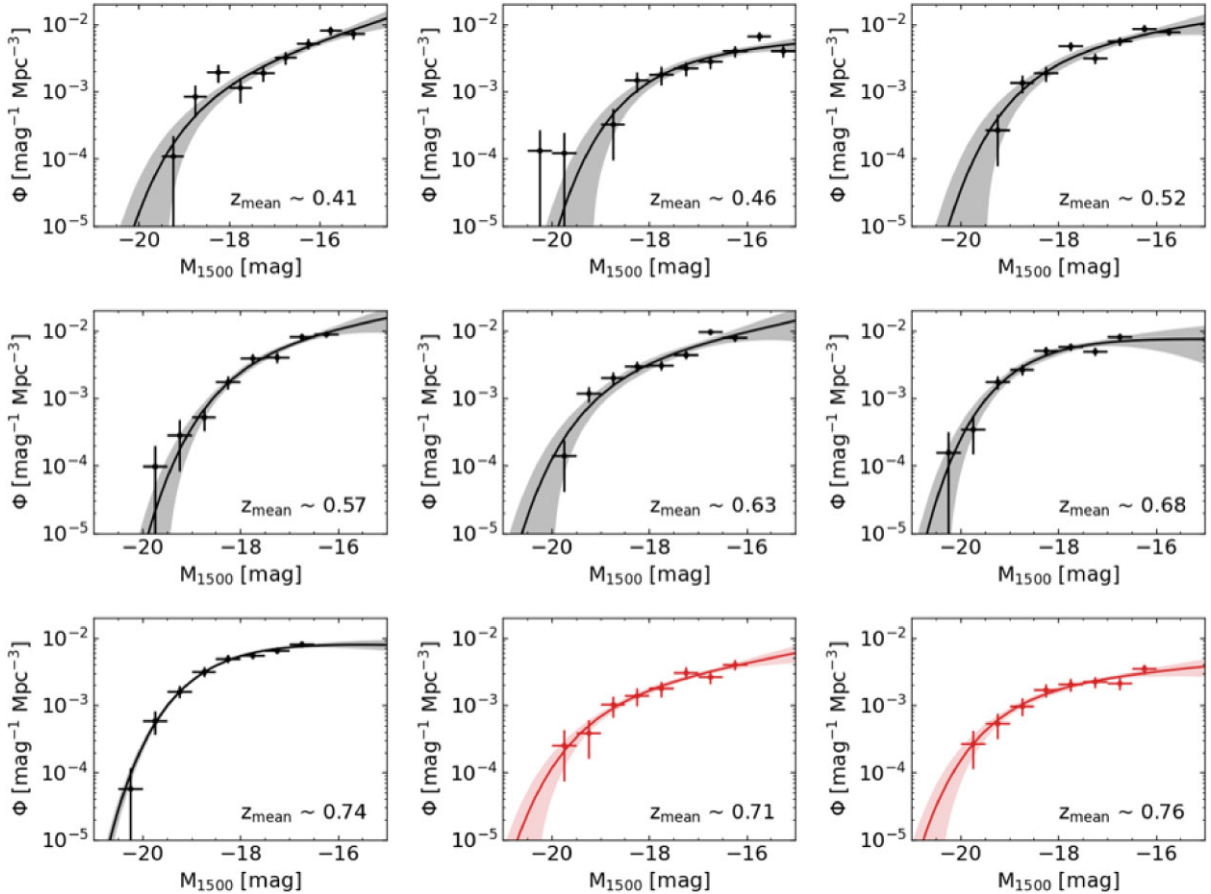
Figure 2. The 1500 Å LF from AstroSat/N242W images of the GOODS-S field in seven different redshift bins are marked in black. The z_{mean} of each bin is also noted. The Schechter function fits for each bin is marked with a solid black line, with the 1σ uncertainty shaded in grey. The centre and right panels of the bottom row show the 1500 Å LF from *HST* F275W images of the GOODS-S field in two different redshift bins, marked in red. The Schechter function fit for each bin is marked with a solid red line, with the 1 σ uncertainty shaded.

for details). Galaxies are observed down to $M_{1500} = -16$ mag for both the redshift bins, deeper than in the N242W data at the same redshift. The Schechter function is fitted to the UVLF for both redshift bins keeping α, ϕ_*, and M^* as free parameters. The best-fitting parameters are noted in Table 1.

4 DISCUSSION AND INFERENCE

4.1 Consistency with AUDFn

Fig. 3 shows the fitted Schechter function parameters determined in this work from Astrosat/UVIT N242W and *HST* F275W galaxies,
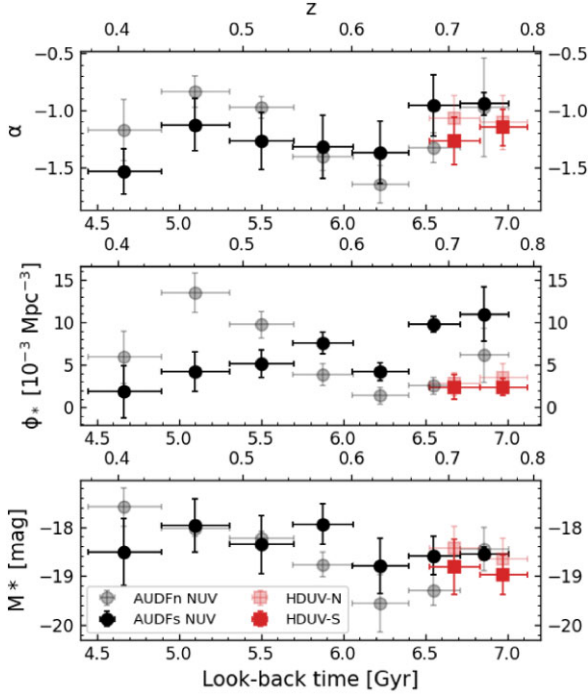
Figure 3. Evolution of the fitted Schechter function parameters with look-back time compared for GOODS-S (this work) and GOODS-N (Bh+24).

compared with those determined in the GOODS-N region for galaxies identified with the same filters by Bh+24. For the *HST* F275W galaxies, UVLFs for HDUV-S and HDUV-N (in the GOODS North region) give consistent fitted Schechter function parameters within error for both redshift bins. For the N242W galaxies for α and M^*, there is consistency within error in these determined parameters across the seven redshift bins.

In the redshift range $0.378 < z < 0.768$ probed here, the lowest fitted α value is at $z_{mean} = 0.41$. For GOODS-N, the galaxies in this redshift bin were found to have a lower mean stellar mass ($\sim 10^{8.5}$ M$_\odot$ (Bh+24)) than those in the higher redshift bins with mean stellar mass $\sim 10^9$ M$_\odot$ (Bh+24). This is also expected to be true for GOODS-S and explains the lower fitted α value, given the presence of star-forming lower mass galaxies.

The apparent dip in α at $z_{mean} = 0.63$ identified in the UVLF parameters fitted to GOODS-N galaxies (Bh+24) is also seen for GOODS-S (see Fig. 3). Comparing the distribution of the determined α values in this work for the seven redshift bins of AUDFs NUV and two redshift bins of HDUV-S (see Table 1) with a normal distribution (having the same mean, $<\alpha> = -1.22$, and standard deviation, $\sigma_\alpha = 0.18$, as the 9 α values) using a Kolmogorov–Smirnov (KS) test (Massey 1951), we obtain a *p*-value > 0.05 (KS-statistic $= 0.155$, *p*-value $= 0.96$) implying the α values may be consistent with a normal distribution. We thus find that while the apparent dip in α at $z_{mean} = 0.63$ may be physical (as this is observed now for both GOODS-S and GOODS-N deep fields), the dip itself is not statistically significant based on the currently available data.

Variations with redshift, similar to that of α, are not seen for ϕ_* and M^*, unlike the case for AUDFn (see Fig. 3), though a seemingly increasing trend is seen for ϕ_* with z, with a noticeable dip at $z_{mean} = 0.63$. The deeper survey likely helps us break the degeneracies between the different fitted Schechter parameters.

There is however a discrepancy in the fitted ϕ_* values with those determined from fitting AUDFn galaxies being higher than those determined from fitting AUDFs galaxies at $z_{mean} = 0.46$ and 0.52, while the opposite is true for $z_{mean} = 0.57$–0.74.

As ϕ_* is the normalization term for the Schechter function fit, it relates closely to the number of galaxies observed in any redshift window. If we restrict the GOODS-S N242W galaxies to only those brighter than 27.05 mag (50 per cent completeness limit of the shallower AUDFn NUV images; Bh+24), the numbers of galaxies are similar to that in GOODS-N field for the $z_{mean} = 0.57$–0.74 redshift bins. The additional survey depth for AUDFs reveals a higher number of fainter galaxies at these redshift bins than anticipated from their UVLF fits, leading to higher fitted ϕ_* values, but this is not as impactful for lower redshift bins.

It is surprising to find that in the redshift bin with $z_{mean} = 0.46$, there are almost ~ 50 per cent more galaxies in GOODS-N than GOODS-S, while the former is the shallower surveyed field. Yantovski-Barth et al. (2024) have identified a number of galaxy clusters in the DESI legacy survey (Dey et al. 2019) images. There is one at $z = 0.4687$ in the GOODS-N field and one more at $z = 0.4834$ centred just beyond this field. Members of both these clusters may be inflating the identified number of galaxies, and hence the determined ϕ_* in the $z_{mean} = 0.46$ redshift bin for GOODS-N. While most cluster members would be passive, it is surprising to see such a noticeable effect in the numbers of GOODS-N NUV sources, which are all expected to be star-forming. We will explore clusters in the AUDFs and AUDFn fields in detail in a future publication.

4.2 Consistency with past determinations of the UVLF

Fig. 4 shows the variation of the three Schechter function parameters, α, ϕ_*, and M^*, with redshift in this work, as well as other direct determinations of these parameters up to $z \sim 1$ from the literature. At the lowest redshift ($z \sim 0.1$) for the UVLF from AstroSat/F154W, the determined α value is more negative than that determined in the GOODS-N field by Bh+24 and by Arnouts et al. (2005) from *GALEX*. However, the ϕ_* values are consistent across all three surveys.

The α and M^* values determined from HDUV-S are consistent with that determined for the highest redshift bin from AUDFs (see Table 1) but the ϕ_* value is lower. This is likely the same effect of the shallower survey depth that also affected the ϕ_* values of the highest redshift bins in AUDFn. Combined with the lack of completeness correction, this effect seems more pronounced leading to low ϕ_* values. Using the same *HST* F275W and also the F435W filters but for a larger area of ~ 426 sq. arcmin and a 5σ detection limit of 27 mag, Sun et al. (2024) presented the UVLF at $z \sim 0.6$–0.8 and $z \sim 0.8$–1, respectively. For all three fitted Schechter function parameters, our determined values at $z_{mean} = 0.68$ and 0.74 are in good agreement with their determination at $z \sim 0.6$–0.8 (see Fig. 4).

Additionally, the XMM-OM based UVLF parameters for $z = 0.6$–0.8 determined for the COSMOS field by Sharma et al. (2024) are also consistent with all three fitted Schechter function parameters at the same highest redshift bins (see Fig. 4). Other parameter determinations from fitting the UVLF to relatively shallower data from different works (Arnouts et al. 2005; Oesch et al. 2010; Sharma et al. 2022), still results in some parameters that agree within error with that from AUDFs, though the ϕ_* values are generally lower for these works (see Fig. 4). The fitted M^* values from Arnouts et al. (2005) are also much lower.
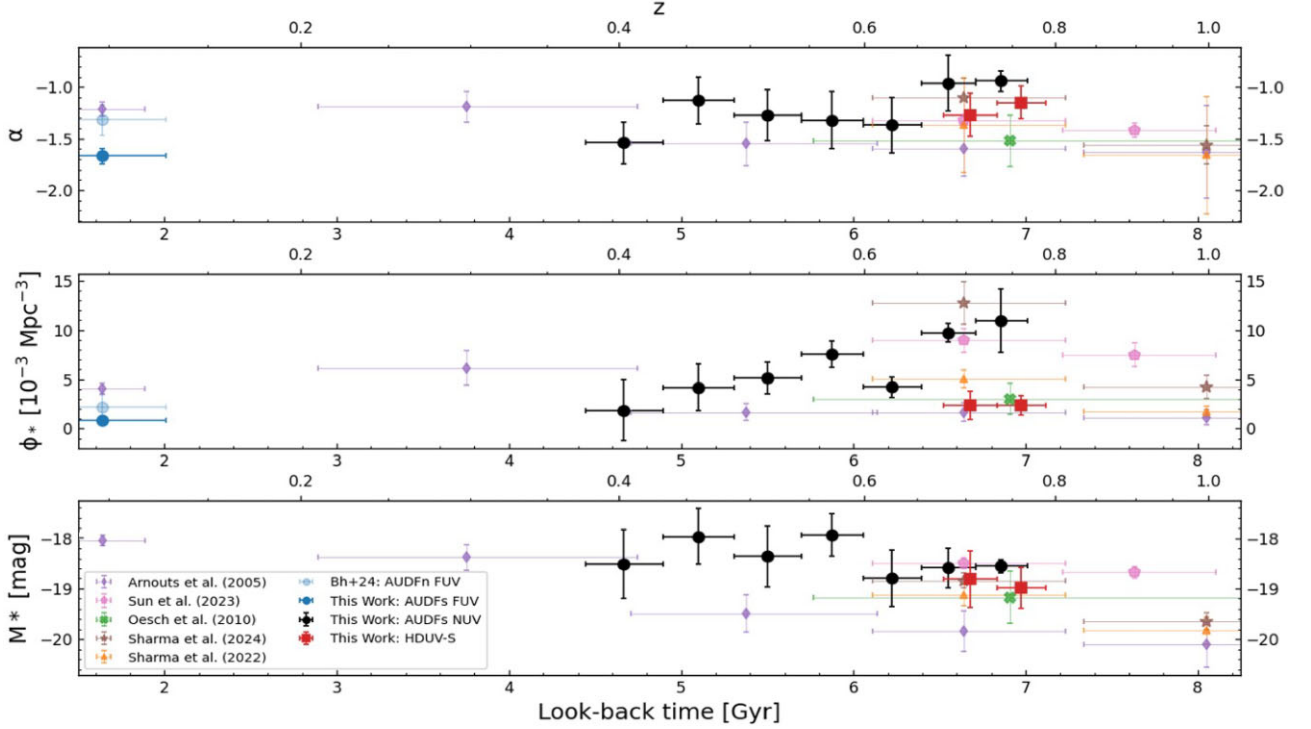
Figure 4. Evolution of the fitted Schechter function parameters with look-back time (bottom axes) and redshift (top axes). The parameters from this work and from literature estimates are marked separately.

4.3 Evolution of the UV luminosity density with redshift

We determine the UV luminosity density for each UVLF determined in this work for the GOODS-S region (by integrating them down to $M_{1500} = -10$). Its logarithm values, $\log(\rho_{UV})$, are noted in Table 1 and plotted against redshift in Fig. 5. We note that the trend in α (Fig. 4), dipping at $z_{mean} = 0.63$ for both GOODS-S (this work) and GOODS-N fields (Bh+24), does not reflect on the $\log(\rho_{UV})$ distribution with redshift, which shows a increasing trend with increasing redshift. The redshift variations of M^* and ϕ_* thus balance the trend in α such that $\log(\rho_{UV})$ trend with redshift does not show any increased star-formation at $z_{mean} = 0.63$.[2] The potential of such a short-lived instance of increased star-formation was discussed in detail in Bh+24.

We additionally determine $\log(\rho_{UV})$ for the lower redshift UVLFs presented by other aforementioned works from their reported fitted parameters, including those from Oesch et al. (2010) and Arnouts et al. (2005) that go out to $z \sim 3$. We also determine $\log(\rho_{UV})$ from the reported parameters of some other works where UVLFs are determined at higher redshifts, i.e. Alavi et al. (2016): $z \sim 1$–3, Parsa et al. (2016): $z \sim 1.8$–4, Atek et al. (2018): $z \sim 6$, Finkelstein et al. (2015): $z \sim 4$–8, Finkelstein et al. (2024): $z \sim 9$–11, and Bouwens et al. (2022): $z \sim 3$–8. While a number of authors have determined the 1500 Å LF at $z > 3$ in recent years, the aforementioned works are those that determined the UVLF down to the greatest observed depths for their presented redshifts. We note that the UVLF beyond $z \sim 8$ is not well-constrained (Bouwens et al. 2023).

Fig. 5 shows the redshift evolution of $\log(\rho_{UV})$. The highest $\log(\rho_{UV})$ values are seen at $z \sim 2.5$ (Arnouts et al. 2005; Oesch et al. 2010; Alavi et al. 2016) with decreasing $\log(\rho_{UV})$ values computed at both higher and lower redshift values as we move away from cosmic noon. Akin to previous authors (Oesch et al. 2010; Alavi et al. 2016), we fit a power-law to the ρ_{UV} values out to $z = 2.6$, which is defined as follows:

$$\rho_{UV} = N \times (1 + z)^\beta, \tag{2}$$

where β is the power-law exponent and N is the normalization constant. The fit is carried out using orthogonal distance regression (Boggs & Rogers 1990), accounting for error in ρ_{UV} and the redshift bin-width as the uncertainty in z. The best-fitting power-law is shown in Fig. 5 with $N = 25.34 \pm 0.06$ erg/s/Hz/Mpc^3 and $\beta = 2.46 \pm 0.2$. This is consistent within errors with $\beta = 2.58 \pm 0.15$ determined by Oesch et al. (2010), but steeper than $\beta = 1.74$ determined by Alavi et al. (2016), as evident in Fig. 5.

Madau & Dickinson (2014, hereafter MD14) defined a modified double-power law function to describe star-formation rate density over the entire range of redshifts. This function was modified by Alavi et al. (2016) to instead describe the equivalent ρ_{UV} values. The function is defined as follows:

$$\rho_{UV} = a \times \frac{(1 + z)^b}{1 + [(1 + z)/d]^c}, \tag{3}$$

where a, b, c, and d are associated with the normalization, rising exponent at low redshift, peak of ρ_{UV}, and falling exponent at high redshift, respectively. The best-fitting MD14 function is shown in Fig. 5 with $a = 25.35 \pm 0.07$, $b = 2.44 \pm 0.21$, $c = 6.29 \pm 0.36$, and $d = 4.44 \pm 0.26$. The normalization and rising exponent are nearly identical to that determined from the power-law fit and consequently the MD14 function fit overlaps with the power-law fit at $z < 2$ (see Fig. 5). Alavi et al. (2016) also fitted the MD14

---

[2]$\log(\rho_{UV})$ is still the highest at $z_{mean} = 0.63$ for the GOODS-N field (see Fig. 5) as noted in Bh+24 but that is a reflection of the lower ϕ_* values at higher z for the shallower GOODS-N survey, as discussed in Section 4.1.
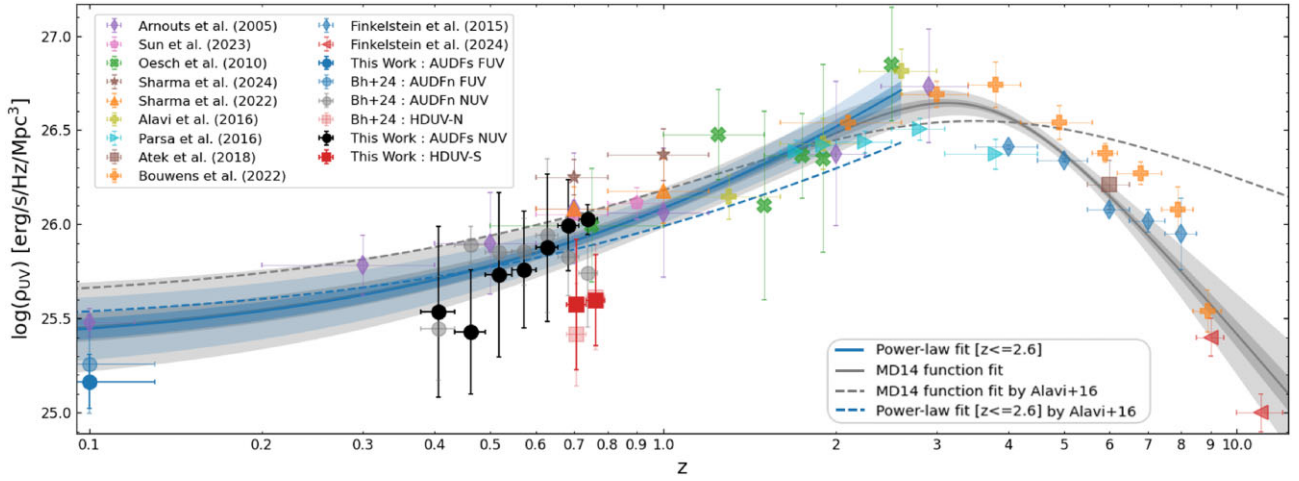
Figure 5. Evolution of the fitted UV luminosity density with redshift (shown in log scale). The best-fitting power-law out to $z = 2.6$ is marked in blue with its 1σ and 3σ bounds marked with darker and lighter shaded regions. The best-fitting MD14 function for the entire redshift range is similarly marked in grey. The same functions with fitted parameters previously determined by Alavi et al. (2016) are also marked.

function (see Fig. 5) with a higher normalization and both rising and falling exponents being less steep. Our determined power-law and MD14 function fits at $z<3$ are now consistent with each-other, compared to the previous determination. Through the availability of additional log ($\rho_{\rm UV}$) determinations at $z > 3$, we better constrain the falling exponent of the MD14 function with increasing redshift.

5 CONCLUSION

Including the UVLF parameters determined in this work, we find that the log($\rho_{\rm UV}$) slope as a function of z (see Fig. 5) at $z <3$ is steeper than the previous best determination by Alavi et al. (2016). This implies that star-formation decline from cosmic dawn to present day was more rapid than the previous estimate by Alavi et al. (2016). We find consistent power-law and MD14 functional fits of the log($\rho_{\rm UV}$) trend with redshift at $z <3$. At $z >3$, by including the literature UVLF parameters obtained out to $z \sim 10$, we find the falling log($\rho_{\rm UV}$) slope is significantly steeper than previous determinations. This implies that star-formation increase till cosmic dawn was also more rapid than the previous estimates.

Cosmic star-formation thus peaked at $z \sim 3$ (see peak of MD14 functional fit in Fig. 5) where-after star-formation has decreased till its present quiescent phase (see also Förster Schreiber & Wuyts 2020, and references therein). To better probe the presence of any short-lived global fluctuations of star formation superimposed on its slow decline since cosmic noon, the UVLF needs to be determined with similarly fine high redshift bins, as achieved in this work, in other observed patches of the universe and at even higher redshifts.

use of ASTROPY – a community-developed core PYTHON package for Astronomy (Astropy Collaboration 2013), SCIPY (Virtanen et al. 2020), NUMPY (Oliphant 2015), and MATPLOTLIB (Hunter 2007). This research also made use of NASA's Astrophysics Data System (ADS).[3]

DATA AVAILABILITY

The AUDFs source catalogue used in this work has already been published by Saha et al. (2024). The HDUV survey catalogue has been published by Oesch et al. (2018). The CANDELS photometric redshift catalogue has been published by Kodra et al. (2023).

REFERENCES

Alavi A. et al., 2016, ApJ, 832, 56
Arnouts S. et al., 2005, ApJ, 619, L43
Astropy Collaboration, 2013, A&A, 558, A33
Atek H., Richard J., Kneib J.-P., Schaerer D., 2018, MNRAS, 479, 5184
Bhattacharya S., Arnaboldi M., Hartke J., Gerhard O., Comte V., Mc-Connachie A., Caldwell N., 2019, A&A, 624, A132
Bhattacharya S., Mishra I., Vaidya K., Chen W. P., 2017, ApJ, 847, 138
Bhattacharya S., Saha K., Mondal C., 2024, MNRAS, 532, 1059 (Bh+24)
Boggs P. T., Rogers J. E., 1990, Contemp. Math., 112, 183
Bouwens R. J. et al., 2023, MNRAS, 523, 1036
Bouwens R. J., Illingworth G., Ellis R. S., Oesch P., Stefanon M., 2022, ApJ, 940, 55
Dey A. et al., 2019, AJ, 157, 168
Finkelstein S. L. et al., 2015, ApJ, 810, 71
Finkelstein S. L. et al., 2024, ApJ, 969, L2
Förster Schreiber N. M., Wuyts S., 2020, ARA&A, 58, 661
Giavalisco M. et al., 2004, ApJ, 600, L93
Grogin N. A. et al., 2011, ApJS, 197, 35
Hagen L. M. Z., Hoversten E. A., Gronwall C., Wolf C., Siegel M. H., Page M., Hagen A., 2015, ApJ, 808, 178
Hunter J. D., 2007, Comput. Sci. Eng., 9, 90
Johnston R., 2011, A&AR, 19, 41
Kodra D. et al., 2023, ApJ, 942, 36
Koekemoer A. M. et al., 2011, ApJS, 197, 36

[3]https://ui.adsabs.harvard.edu

Kumar A. et al., 2012, in Takahashi T., Murray S. S., den Herder J.-W. A., eds, Proc. SPIE Conf. Ser. Vol. 8443, Space Telescopes and Instrumentation 2012: Ultraviolet to Gamma Ray. SPIE, Bellingham, p. 84431N

Lyu J., Alberts S., Rieke G. H., Rujopakarn W., 2022, ApJ, 941, 191

Madau P., Dickinson M., 2014, ARA&A, 52, 415 (MD14)

Massey F. J., 1951, J. Am. Stat. Assoc., 46, 68

Mondal C. et al., 2023, ApJS, 264, 40

Oesch P. A. et al., 2010, ApJ, 725, L150

Oesch P. A. et al., 2018, ApJS, 237, 12

Oke J. B., 1974, ApJS, 27, 21

Oliphant T. E., 2015, Guide to NumPy, 2nd edn. CreateSpace Independent Publ. Platform, USA

Page M. J. et al., 2021, MNRAS, 506, 473

Page M. J., Carrera F. J., 2000, MNRAS, 311, 433

Parsa S., Dunlop J. S., McLure R. J., Mortlock A., 2016, MNRAS, 456, 3194

Saha K. et al., 2024, ApJS, 275, 28

Schechter P., 1976, ApJ, 203, 297

Sharma M., Page M. J., Breeveld A. A., 2022, MNRAS, 511, 4882

Sharma M., Page M. J., Ferreras I., Breeveld A. A., 2024, MNRAS, 531, 2040

Singh K. P. et al., 2014, in Takahashi T., den Herder J.-W. A., Bautz M., eds, Proc. SPIE Conf. Ser. Vol. 9144, Space Telescopes and Instrumentation 2014: Ultraviolet to Gamma Ray. SPIE, Bellingham, p. 91441S

Sullivan M., Treyer M. A., Ellis R. S., Bridges T. J., Milliard B., Donas J., 2000, MNRAS, 312, 442

Sun L. et al., 2024, ApJ, 972, 8

Tandon S. N. et al., 2020, AJ, 159, 158

Treyer M. A., Ellis R. S., Milliard B., Donas J., Bridges T. J., 1998, MNRAS, 300, 303

Virtanen P. et al., 2020, Nat. Methods, 17, 261

Wyder T. K. et al., 2005, ApJ, 619, L15

Yantovski-Barth M. J., Newman J. A., Dey B., Andrews B. H., Eracleous M., Golden-Marx J., Zhou R., 2024, MNRAS, 531, 2285

This paper has been typeset from a TeX/LaTeX file prepared by the author.